VIBRATORY LOADS REDUCTION TESTING OF THE NASA/ARMY/MIT ACTIVE TWIST ROTOR

Matthew L. Wilbur
m.l.wilbur@larc.nasa.gov

Paul H. Mirick
p.h.mirick@larc.nasa.gov

William T. Yeager, Jr.
w.t.yeager@larc.nasa.gov

Chester W. Langston
c.w.langston@larc.nasa.gov

Army Research Laboratory
NASA Langley Research Center
Hampton, VA 23681

Carlos E. S. Cesnik
ccesnik@mit.edu

SangJoon Shin
ssjoon@mit.edu

Active Materials and Structures Laboratory
Massachusetts Institute of Technology
Cambridge, MA 02139

ABSTRACT

Recent studies have indicated that controlled strain-induced blade twisting can be attained using piezoelectric active fiber composite technology, and that such advancement may provide a mechanism for reduced rotorcraft vibrations and increased rotor performance. In order to validate these findings experimentally, a cooperative effort between the NASA Langley Research Center, the Army Research Laboratory, and the MIT Active Materials and Structures Laboratory has been developed. As a result of this collaboration a four-bladed, aeroelastically-scaled, active-twist model rotor has been designed and fabricated for testing in the heavy gas test medium of the NASA Langley Transonic Dynamics Tunnel. Initial wind tunnel testing has been conducted to assess the impact of active blade twist on both fixed- and rotating-system vibratory loads in forward flight. The active twist control was found to have a pronounced effect on all system loads and was shown to generally offer reductions in fixed-system loads of 60% to 95%, depending upon flight condition, with 1.1º to 1.4º of dynamic blade twist observed. A summary of the systems developed and the vibratory loads reduction results obtained are presented in this paper.

INTRODUCTION

Rotorcraft vibration and noise reduction, as well as increasing rotor performance and maneuverability, continue to be a primary concern of the rotorcraft research community. One promising means of attaining such goals is to define an efficient way to achieve helicopter rotor individual blade control without the need for hydraulic power in the rotating system. Numerous electromechanical approaches exploiting active (smart) material actuation mechanisms have been investigated for this purpose.[1] The most widely explored active material actuation methods have employed either piezoelectrically actuated flaps placed at discrete locations along the blade,[2-9] or piezoelectric material distributed along the blade and used to directly control deformations (usually twist) in the host blade structure.[9-19] The primary design constraint in both approaches is the need to obtain high piezoelectric actuation forces and displacements with a minimum of actuator weight. An additional concern with flap actuation mechanisms is that they must be designed to fit within the geometric confines of the blade structure. Direct control of blade twisting using embedded piezoelectric materials, although simple conceptually, has proven to be difficult to implement with conventional piezoelectric materials. Over the past five years, however, piezoelectric active fiber composite (AFC) actuators have been shown to have the proper combination of conformability and performance characteristics necessary to develop a useful individual blade control system.[9, 12-19]

The active fiber composite actuator utilizes interdigitated electrode (IDE) poling and piezoelectric fiber composites (PFC), which result in a high performance piezoelectric actuator laminate with strength and conformability characteristics greater than that of a conventional monolithic piezoceramic.[20] In particular, the high conformability of the actuator package allows it to be embedded easily within nonplanar structures, much like a traditional composite ply.

Presented at the American Helicopter Society 57th Annual Forum, Washington, DC, May 9-11, 2001.

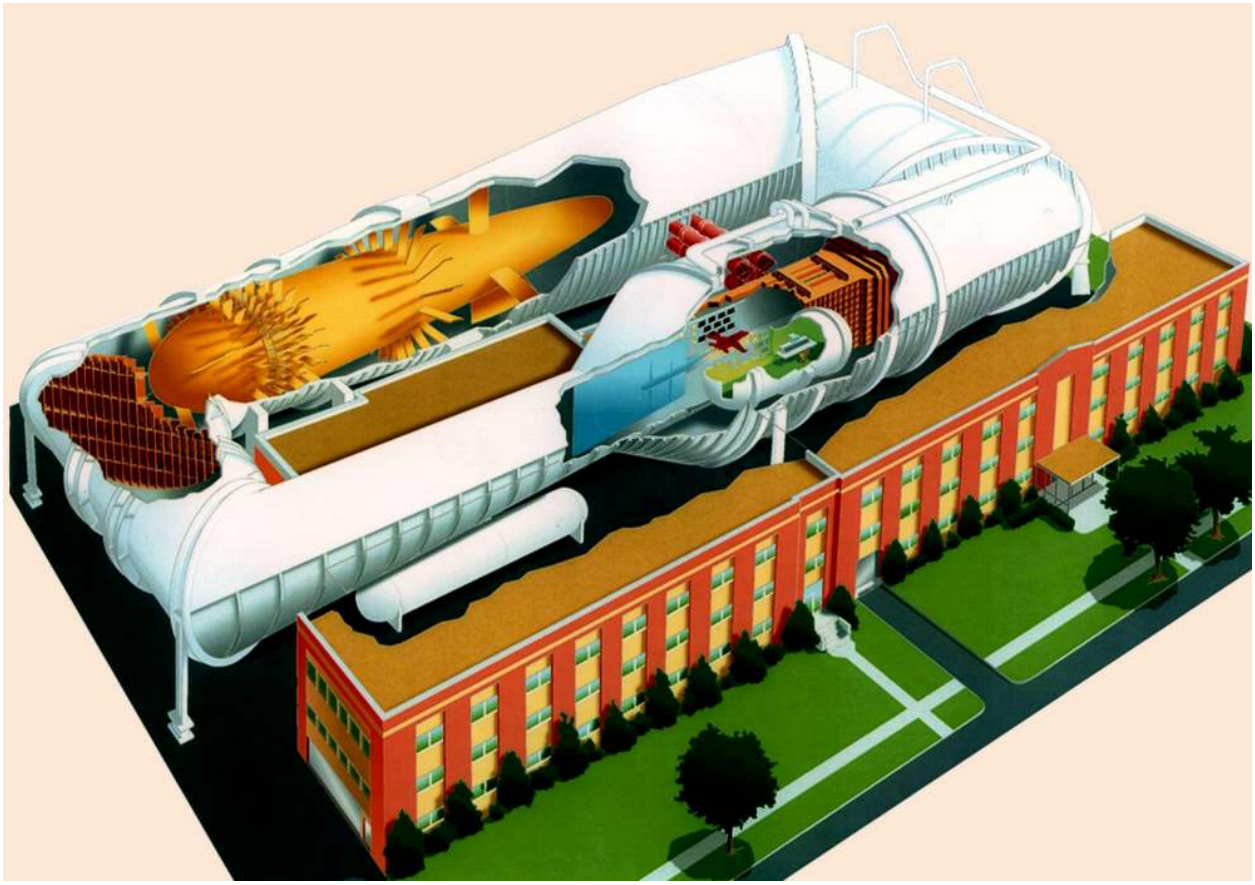

Figure 1. The Langley Transonic Dynamics Tunnel (TDT).

A cooperative effort between the NASA Langley Research Center, the Army Research Laboratory, and the MIT Active Materials and Structures Laboratory has been developed to perform initial feasibility and proof-of-concept studies of active twist rotor (ATR) technologies. The goal of the ATR program is to provide a wind-tunnel demonstration of an active fiber composite active twist rotor concept and to investigate the potential benefits of such a system to reduce rotorcraft vibrations and noise, and, to a lesser extent, investigate potential improvements in rotor performance. This is being accomplished using a 110-inch diameter aeroelastically-scaled wind-tunnel model rotor designed for testing in the heavy gas, variable density test medium of the NASA Langley Transonic Dynamics Tunnel (TDT)[21]. The TDT is a unique facility in that it permits full-scale rotor tip Mach numbers, Froude numbers, and Lock numbers to be matched simultaneously at model scale. In particular, the reduced speed of sound in the heavy gas test medium allows full-scale tip Mach numbers to be matched at lower rotational speeds and drive motor power.

The design, fabrication, and preliminary bench and hover testing of a prototype Active Twist Rotor blade has been completed, and the results reported in references 15 through 18. Recently, forward-flight testing has been conducted in the Transonic Dynamics Tunnel to assess the impact of active twist on rotating- and fixed-system vibratory loads and acoustic noise generation. This paper will provide a summary of the systems used and the vibratory loads results obtained during testing.

APPARATUS AND PROCEDURES

Wind Tunnel

The Langley Transonic Dynamics Tunnel, shown in figure 1, is a continuous-flow pressure tunnel capable of speeds up to Mach 1.2 at stagnation pressures up to 1 atm. The TDT has a 16-ft square slotted test section that has cropped corners and a cross-sectional area of 248 ft^2. Either air or R-134a, a heavy gas, may be used as the test medium. The TDT is particularly suited for rotorcraft aeroelastic testing primarily because of three advantages associated with the heavy gas. First, the high density

of the test medium allows model rotor components to be heavier; thereby more easily meeting structural design requirements while maintaining dynamic scaling. Second, the low speed of sound in R-134a (approximately 550 ft/sec) permits much lower rotor rotational speeds to match full-scale hover tip Mach numbers and reduces the time-scales associated with active control concepts and dynamic response. Finally, the high-density environment increases the Reynolds number throughout the test envelope, which allows more accurate modeling of the full-scale aerodynamic environment of the rotor system. Hover and forward-flight testing of the ATR was conducted in the heavy gas test medium at a constant density of 0.0047 sl/ft^3.

Model Description

Testbed. The Aeroelastic Rotor Experimental System (ARES) helicopter testbed, shown in figures 2 and 3, was used for all hover and forward-flight testing. The ARES is powered by a variable-frequency synchronous motor rated at 47-hp output at 12,000 rpm. The motor is connected to the rotor shaft through a belt-driven, two-stage speed-reduction system. Rotor control is achieved by a conventional hydraulically-actuated rise-and-fall swashplate using three independent actuators. Similarly, rotor-shaft angle of attack is controlled by a single hydraulic actuator.

Instrumentation on the ARES testbed permits continuous display of model control settings, rotor speed, rotor forces and moments, fixed-system accelerations, blade loads and position, and pitch-link loads. All rotating-system data are transferred through a 30-channel slip ring assembly to the testbed fixed system. An additional slip ring permits the transfer of high-voltage power from the fixed system to the rotating system for actuation of the AFC actuators embedded in the ATR blades. A six-component strain-gage balance placed in the fixed system 21.0 inches below the rotor hub measures rotor forces and moments. The strain-gage balance supports the rotor pylon and drive system, pitches with the model shaft, and measures all of the fixed-system forces and moments generated by the rotor model. A streamlined fuselage shape encloses the rotor controls and drive system; however, the fuselage shape is isolated from the rotor system such that its forces and moments do not contribute to the loads measured by the balance.

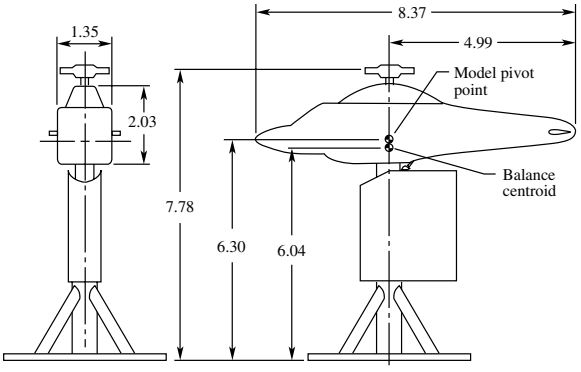

Figure 2. Schematic of the Aeroelastic Rotor Experimental System (ARES) helicopter testbed. All dimensions are in feet.

Figure 3 shows the Active Twist Rotor mounted on the ARES helicopter testbed in the TDT. For this configuration a four-bladed articulated hub with coincident flap and lag hinges is used on the ARES. The pitch bearing for the hub is located outboard of the flap and lag hinges, and trailing pitch links are used. The hub is configured such that pitch-flap coupling of 0.5 (flap up, pitch down) is obtained and the lag-pitch coupling is minimized.

ATR Blades. Each ATR blade utilizes 24 active fiber composite (AFC) actuators to implement the active twist control of each blade. The AFC actuators, shown conceptually in figure 4, are embedded directly in the structure of each blade D-spar, spanning from 0.30R (30% blade radius) to 0.98R. The AFCs are placed in four layers through the thickness of the blades and are oriented such that the active strain is applied at ±45º relative the blade spanwise axis to permit maximum torsional control of the blades. Actuation of the AFCs is accomplished using separate high-voltage, low-current power channels for each blade. A jumper board mounted on top of the ARES articulated hub permits electrical connections to the individual AFCs on the blades and serves as a distribution center for the power channels delivered by the high-voltage slip ring.

Figure 3. The ARES testbed in the TDT with the ATR hardware installed.

Table 1. Active Twist Rotor General Parameters

Property	Description	Value
$\boldsymbol{R}$	Blade radius, ft	4.583
c	Blade chord, ft	0.353
r_c	Root cutout, ft	1.04
θ_{pt}	Blade linear pretwist, deg	-10.0
$\boldsymbol{N}$	Number of blades	4
e	Flap-lag hinge location, ft	0.25
Ω_0	Nominal rotor rotational speed, rpm	688
ρ_0	Nominal test medium density, sl/ft^3	0.0047
M_{tip}	Blade hover tip Mach number	0.60
T_{1g}	Rotor thrust for simulated 1g flight, lb	225.0

The ATR blades, general parameters for which are provided in Table 1, have a rectangular planform with a chord of 4.24 inches, radius of 55.0 inches, and a NACA-0012 airfoil section. Pretwist is linear with a twist of –10° from the center of rotation to the blade tip. Instrumentation on the ATR blades consists of ten 4-arm strain-gage bridges. Of these, six bridges measure torsion moments, three bridges measure flapwise bending moments, and one bridge measures chordwise bending moments. Table 2 lists the location and the designation used for each gage throughout the paper. Prior to testing the two outboard flap gages (F2 and F3) were determined to be inoperative.

Additional instrumentation on the ATR blades includes accelerometers mounted chordwise along the 0.98R spanwise station. The accelerometers are embedded in the blade structure, centered about the blade quarter-chord, sense accelerations in the flap bending direction, and are calibrated to provide an indication of blade dynamic twist.

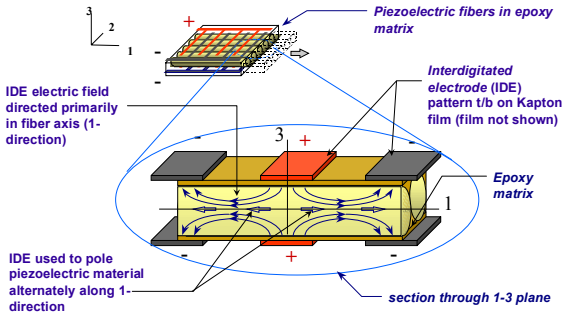

Figure 4. Active Fiber Composite (AFC) piezoelectric actuator concept.

Table 2. ATR Blade Strain Gage Bridges

Designation	Blade Station, in	Blade Station, r/R	Orientation
T1	18.5	0.336	Torsion
T2	24.6	0.447	Torsion
T3	30.7	0.558	Torsion
T4	36.8	0.669	Torsion
T5	42.9	0.780	Torsion
T6	49.0	0.891	Torsion
F1	15.8	0.287	Flap
F2	25.5	0.464	Flap[1]
F3	44.5	0.809	Flap[1]
C1	15.8	0.287	Chord

[1]Inoperative

ATR Computer Control System

Active-twist control of the ATR blades is achieved with a computer control system incorporating a digital signal processor board, 32 analog-to-digital channels, 6 digital-to-analog channels, and 32 digital input-output channels. The ATR computer control system may be used in two open-loop operating modes, each of which generates prescribed sinusoidal twist excitation voltages for the ATR blades. The first operating mode permits the user to prescribe the voltage amplitude and frequency to be delivered to each of the blades and is useful in acquiring frequency response data with the rotor system. The second operating mode permits the user to prescribe the rotor control type, the voltage amplitude, harmonic frequency, and control phase, and is used most typically during forward-flight testing because the active-twist inputs are synchronized directly with the rotor rotation. Available control types include a collective twist mode where all four blade are twisted simultaneously, and an Individual Blade Control (IBC) mode where each blade twists according to a prescribed schedule associated with its position in the rotor azimuth. For each operating mode the ATR computer control system generates low-voltage, sinusoidal control signals for each blade that are amplified by linear high-voltage amplifiers. To minimize the potential for damage to the AFCs the control system is designed to limit the maximum blade voltage amplitude to 1000 volts, approximately one-half of the AFC maximum design voltage.

The ATR computer control system is also used for real-time monitoring of AFC health, and blade and fixed-system response. Real-time displays are generated that provide user feedback of the actual voltage and current delivered to each blade, the dynamic tip twist of each blade resolved from the on-

blade tip accelerometers, and the 4-per-revolution (4P) response of the fixed system resolved from balance measurements.

Projection Moiré Interferometry System

A Projection Moiré Interferometry[22] (PMI) system was used to perform noninvasive measurements of blade displacement for selected conditions during the test. The PMI system, as applied to measuring rotorcraft blade deformation, is shown conceptually in figure 5. A projection system, aligned such that its optical axis was perpendicular to the upper surface of the blade, was used to project a grid of equi-spaced parallel lines onto the rotor blade. A video camera with a narrow bandpass filter matched to the projector illumination wavelength was positioned to view the model at a 30º to 45º angle inclined from the projector optical axis. Images of the grid lines projected onto the model were acquired using a frame grabber board installed in a PC-compatible computer. These images were processed offline to obtain a quantitative, spatially continuous representation of the model surface shape or deformation. For this test, custom-built conditional sampling electronics were used to count pulses from a 1 pulse-per-revolution encoder and a 64 pulse-per-revolution encoder mounted on the rotor shaft. Based on the encoder counts, the electronics triggered the PMI projection system, camera, and frame grabber to obtain image captures only at azimuthal positions ranging from 157.5º to 225.0º, relative to 0º azimuth over the testbed tail. PMI measurements were made for selected conditions throughout the test and represent the difference in blade displacements between the active twist control on and the control off conditions.

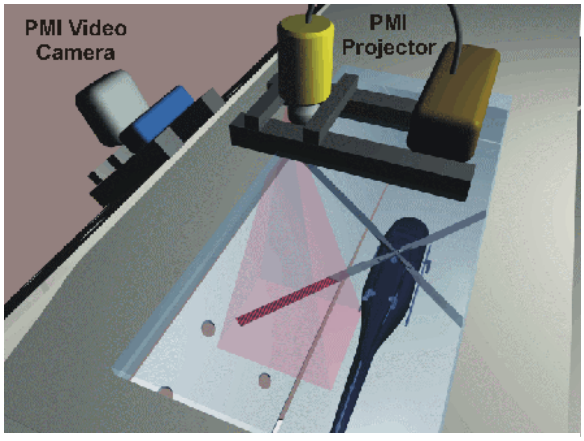

Figure 5. Projection Moiré Interferometry system setup.

Data Acquisition Methods

Data acquisition throughout the test was accomplished using three separate data acquisition computer systems and the ATR computer control system. The primary system used for acquisition of the vibratory loads data was a Modcomp computer with a Neff 600-series, 256-channel, 16-bit analog-to-digital converter with sample-and-hold. Low-pass anti-aliasing filters were set to 200 Hz for each data channel and a sampling rate of 1000 samples-per-second was used. Five seconds of data were typically acquired on the Modcomp computer system for each data point. A subset of the channels processed by the Modcomp system was also sampled by the ATR computer control system. The sampling rate on this system was 4000 samples-per-second, with data acquired for 3 seconds for each data point. Separate data acquisition systems were also utilized to acquire the acoustic noise data and the PMI displacement measurements. Generally, the ATR computer control system was used to initiate data acquisition streams on each of the systems simultaneously.

Test Procedures

All hover and forward-flight testing was conducted in the heavy gas test medium of the TDT at a nominal density of 0.0047 sl/ft^3. The rotor rotational speed throughout the test was held at a constant 688 rpm, resulting in a nominal hover tip Mach number of 0.60. The bulk of the testing was conducted in forward flight with various steady-state trim conditions representative of sustained 1g level flight and descending flight. A rotor lift coefficient of 0.0066 was chosen for the nominal lifting task throughout the test, and the rotor-shaft angle of attack was chosen as a function of flight speed to represent the various flight conditions.

Hover Testing. Testing was conducted in hovering flight to determine the basic frequency response characteristics of the ATR blades under active twist control. Previous testing of an ATR prototype blade indicated that blade pitch had a minimal effect on all frequency response measurements[18]; therefore, all measurements were conducted with the ATR at a collective pitch of 0º. Excitation voltage amplitudes of 250 V, 500 V, 750 V, and 1000 V were tested using sine dwells for discrete frequencies ranging from 1 Hz to 100 Hz, encompassing the frequency range up to approximately 8.7P.

Table 3. ATR Forward Flight Test Matrix

	$\mu = 0.140$	$\mu = 0.170$	$\mu = 0.200$	$\mu = 0.233$	$\mu = 0.267$	$\mu = 0.300$	$\mu = 0.333$	$\mu = 0.367$
$\alpha_s = +8^\circ$	X							
$\alpha_s = +5^\circ$	X							
$\alpha_s = +4^\circ$	X	X	X	X	X			
$\alpha_s = +2^\circ$	X			X	X			
$\alpha_s = +1^\circ$		X						
$\alpha_s = 0^\circ$	X		X	X	X			
$\alpha_s = -1^\circ$	X	X	X					
$\alpha_s = -2^\circ$	X			X	X			
$\alpha_s = -4^\circ$						X	X	
$\alpha_s = -6^\circ$							X	X
$\alpha_s = -8^\circ$							X	

Forward-Flight Testing. Testing was conducted in forward flight to determine the effect of active twist on fixed- and rotating-system vibratory loads and acoustic noise. Table 3 presents the conditions tested in terms of advance ratio, μ, and rotor-shaft angle of attack, α_s. For each condition tested the rotor was set to a rotational speed of 688 rpm, trimmed to a nominal lift coefficient, C_L, of 0.0066, and the first-harmonic blade flapping with respect to the rotor shaft trimmed to within 0.1º.

For each condition tested, data were acquired with active twist control disabled. These sets of data will be referred to throughout the paper as the "baseline" condition. Typically, several sets of baseline data were acquired to establish a set of well-determined baseline loads and conditions. The effect of active twist control was achieved by selecting the type of actuation: collective or IBC twist; the actuation voltage amplitude, typically 500 V, 750 V, or 1000 V; and the harmonic frequency of actuation, typically 3P, 4P, or 5P. Then, the ATR computer control system was used to automatically excite the rotor system with the prescribed amplitude, control type, and frequency parameters at a sequence of control phases beginning with 0º and progressing to 360º in 20º increments. At each control phase increment the control conditions were held, permitting the rotor and fixed-system transient responses to dampen, then data were automatically acquired simultaneously on the ATR computer control system, and the Modcomp and acoustic data acquisition systems. Once the acquisition sequence was completed on each data acquisition system the next control phase increment was set by the ATR computer control system and the data acquisition sequence repeated. This procedure continued until all control phase increments had been completed. In this manner, measurements were made for 19 control phases with the first measurement made at a control phase of 0º with the final measurement in the sequence being a repeat of the first.

It is worth noting that although control phase is indexed by the rotor azimuth (i.e., 0º control phase is coincident with 0º azimuth), control phase is not equivalent to rotor azimuth. This is because there are multiple cycles of blade twist control (either 3, 4, or 5) for each rotor revolution, and the control phase is related to a single cycle of the blade twist control. Thus, the azimuth at which maximum twist control is commanded may be determined by dividing the control phase by the harmonic excitation. For example, a 3P twist actuation with control phase of 180º would impose the maximum twist control at a rotor azimuth of 60º. The second and third cycles would achieve maximum twist control at 180º and 300º, respectively.

RESULTS

The wind-tunnel test of the Active Twist Rotor system was highly successful in that the many complex systems yielded few problems. In particular, the high-voltage system and the ATR blades, previously considered to be the greatest

source of potential difficulties, performed practically flawlessly throughout the test. Of the 96 AFC actuators installed on the four rotor blades, no failures were encountered during more than 40 hours of twist actuation time. Further, initial testing was conducted in hover to determine the frequency response characteristics of the rotor blades under active twist control. Identical testing was repeated at the conclusion of the test, showing that no loss of actuator authority was evident.

The collective twist mode was determined to be relatively ineffective in reducing fixed-system vibratory loads in comparison to the IBC mode of operation. It was also shown that simulated 1g flight conditions generated larger fixed-system vibratory loads (control off) than did the descending (positive shaft angle) flight conditions. Therefore, the results presented in this paper will be limited to those obtained during the simulated 1g flight conditions while in the baseline (control off) or IBC active twist mode of operation.

In general, the testing demonstrated the potential for 60% to 95% reductions in fixed-system vibratory loads due to active twist control in 1g forward flight. Generally, the largest active twist control authority (1000 V) resulted in the greatest impact on fixed- and rotating-system loads. Figures 6 and 7 present an overview of the predominant results of the testing at the two conditions generating the largest 4P fixed-system loads. Figure 6 presents results obtained at $C_L = 0.0066$, $\mu = 0.140$, α_s = -1.0º, and 1000 V active twist actuation. Figure 7 presents results obtained at $C_L = 0.0066$, $\mu = 0.333$, α_s = -6.0º, and 1000 V active twist actuation. Each of the figures present the results of rotating-system loads for the predominant frequencies of interest (3P, 4P, and 5P) and the 4P fixed-system shear loads obtained as a function of active twist control phase. The four rotating-system load plots in figure 6 present the blade flap, chord, and torsion moments measured at the most inboard strain-gage locations (F1, C1, and T1 respectively as identified in Table 2) and the pitch link load. Pitch link results are not presented in figure 7 due to a problem with the slip-ring channel associated with the data during testing. Each of the rotating system plots is presented with "ribbons" representing the changing harmonic blade loads as a function of active twist control phase. The vertical bars on the rear surface of the plots (at 0º control phase) are representative of the harmonic loads generated by the baseline (control off) condition. The three x-y plots at the bottom of each figure present the 4P fixed-system shear load components, considered to be of primary importance, as a function of active twist control phase, with the horizontal line spanning each plot representing the baseline condition. Results are presented in both figures 6 and 7 for active twist actuation at 3P, 4P, and 5P.

Low Advance Ratio ($\mu = 0.140$)

Figure 6(a) presents the results obtained at $C_L = 0.0066$, μ = 0.140, and α_s = -1.0º with 3P, 1000V amplitude active twist actuation. Dramatic variations in both fixed- and rotating-system loads are evident as the twist control phase angle is varied. Of note are the 3P blade flapping moment, which is more than double the baseline load at a control phase of 0º and is virtually eliminated at a control phase of 180º; and the 3P blade torsion moment, which has increased by more than an order of magnitude due to the twist actuation loads. Significant variations are also noted in all three harmonics of the blade chordwise moment, and the 3P and 4P pitch link loads, which are nearly zero at 160º and 200º, respectively. The net effect of the rotating-system loads are observed in the fixed-system as minimum loads in the range of 180º to 220º control phase where reductions of 60% to 90% are evident. The character of the 4P fixed-system side and axial force responses are noted as being similar to that exhibited by the 3P blade chord moment. The reduction in 4P fixed-system normal force was a somewhat unexpected result for 3P twist actuation and is most likely due to a combination of moderate rotating-system load reductions evident in the 4P flapping, chordwise, and pitch link loads. Though not presented in figure 6(a), reductions in 4P fixed-system pitching moment, rolling moment, and yawing moment of 90%, 80%, and 30%, respectively, were also noted in the 180º to 220º control phase range.

Figure 6(b) presents the results obtained at $C_L = 0.0066$, $\mu = 0.140$, and α_s = -1.0º with 4P, 1000 V amplitude active twist actuation. While 4P twist actuation was expected to produce the greatest reduction in 4P fixed-system normal force loads, figure 6(b) clearly indicates the contrary. Although significant reductions are noted in 4P blade flapping and chord moments at 220º twist control phase, an examination of the response phases (not presented) indicates that a five-fold increase in 4P pitch link loads is in opposition to the beneficial responses noted in the blade bending moments, effectively eliminating any potential improvement in the 4P fixed-system normal force response. As with the 3P active twist excitation (figure 6(a)), the 3P blade chord moment appears to be the most significant driver in 4P fixed-system side force response.

Figure 6(c) presents the results obtained at $C_L = 0.0066$, $\mu = 0.140$, and α_s = -1.0º with 5P, 1000 V amplitude active twist actuation. Significant 4P

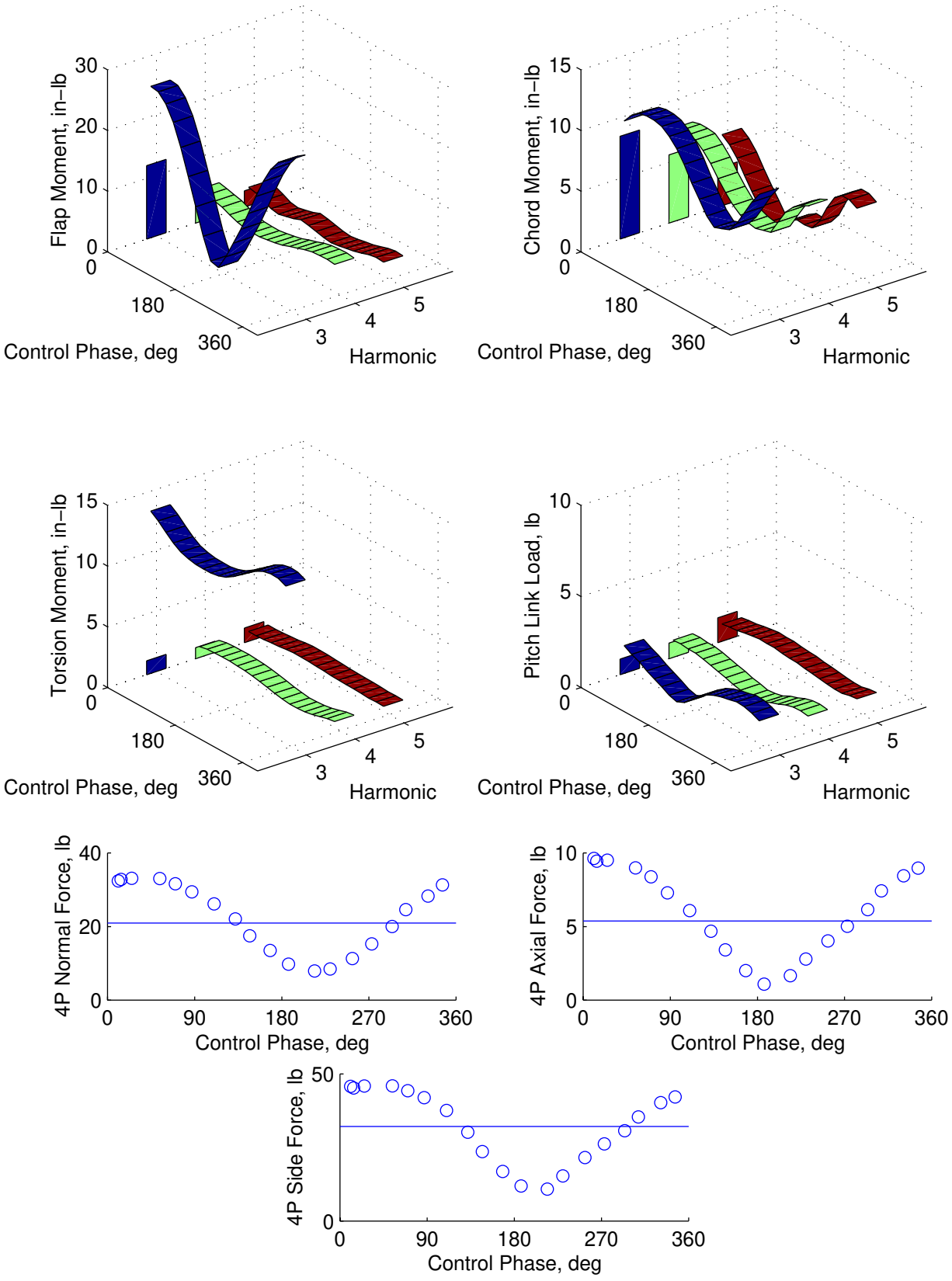

Figure 6(a). Rotating- and fixed-system loads for C_L = 0.0066, μ = 0.140, α_s = -1.0º, and 3P, 1000 V twist actuation.

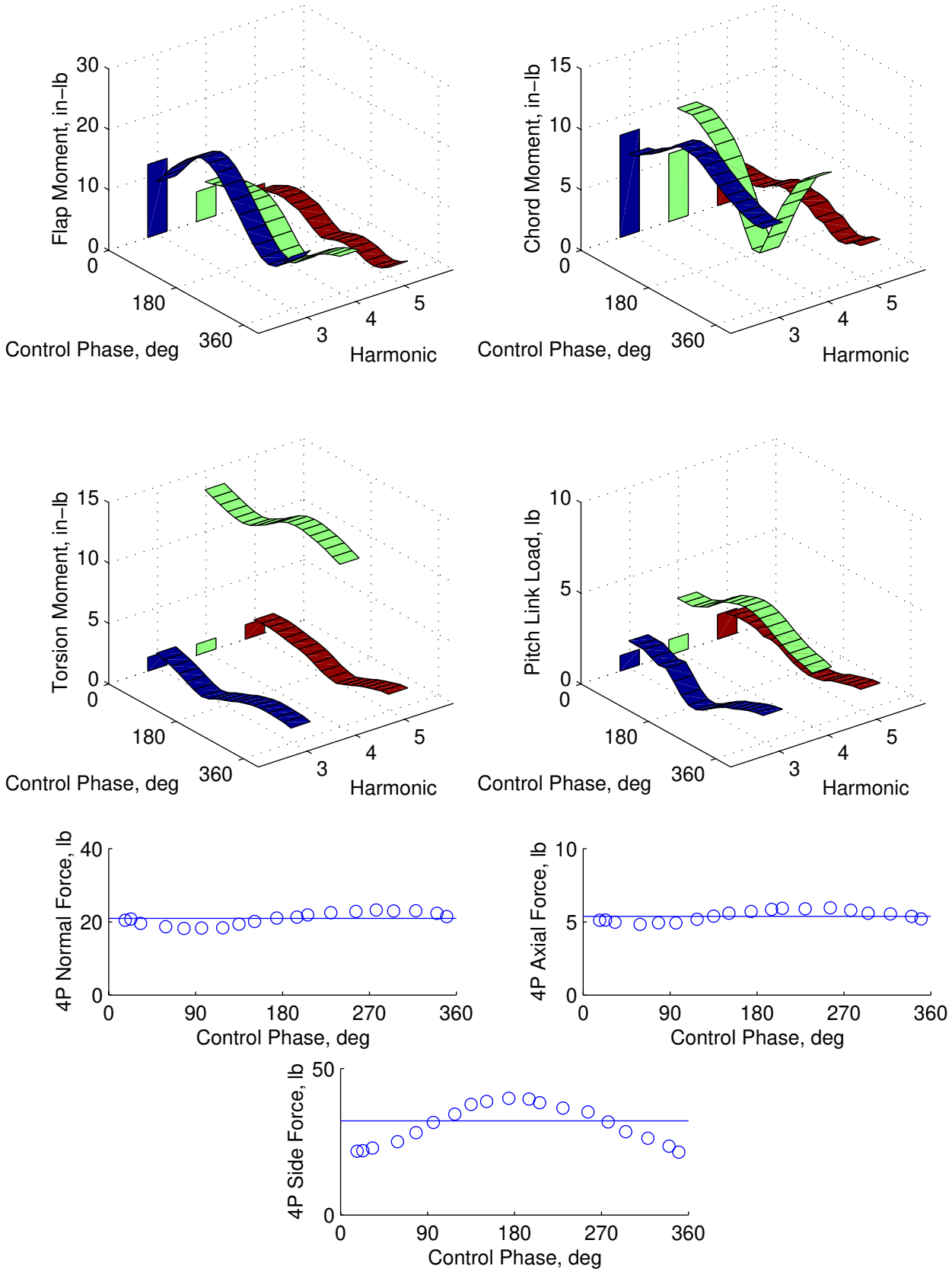

Figure 6(b). Rotating- and fixed-system loads for $C_L = 0.0066$, $\mu = 0.140$, $\alpha_s = -1.0°$, and 4P, 1000 V twist actuation.

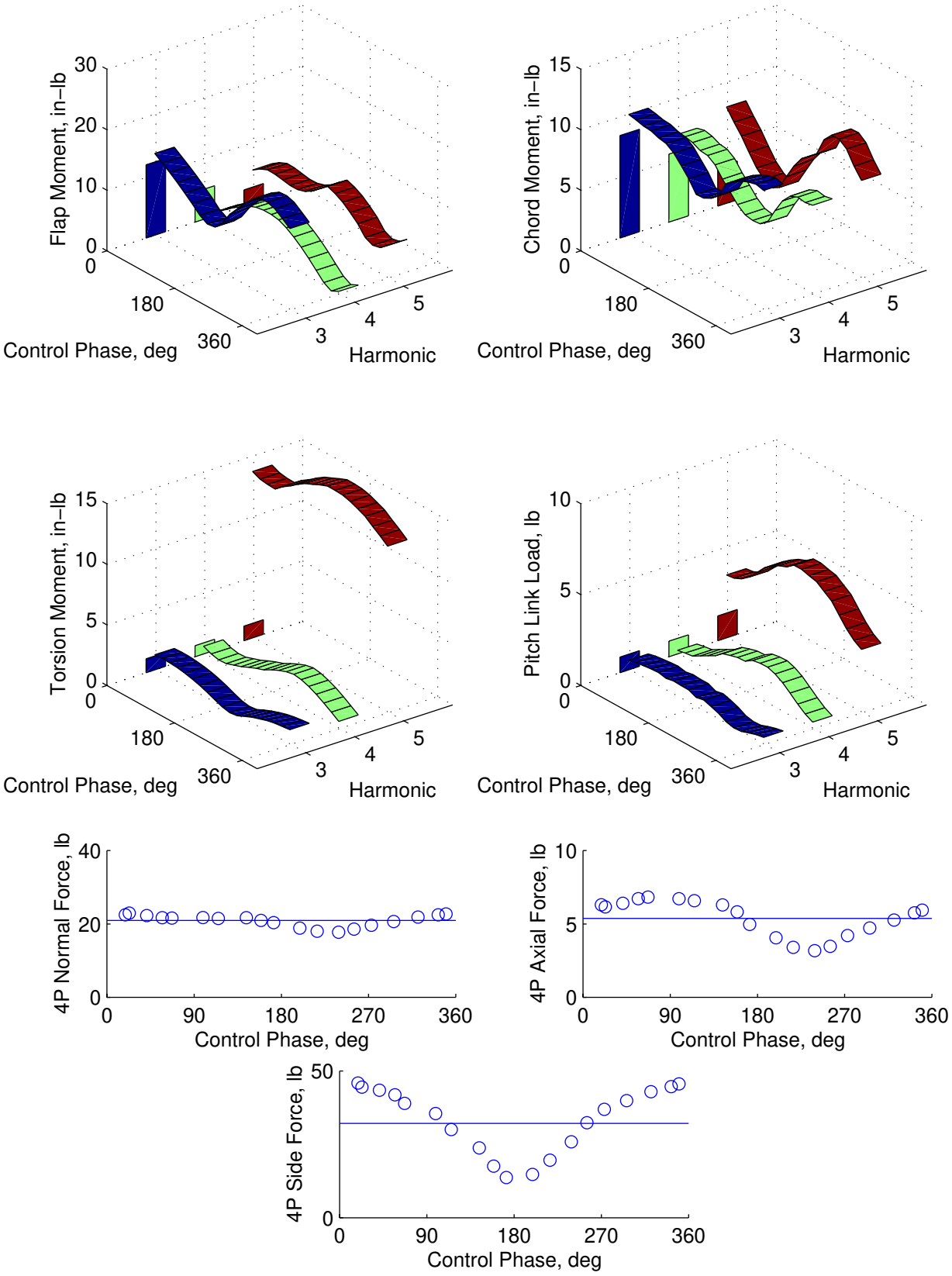

Figure 6(c). Rotating- and fixed-system loads for $C_L = 0.0066$, $\mu = 0.140$, $\alpha_s = -1.0°$, and 5P, 1000 V twist actuation.

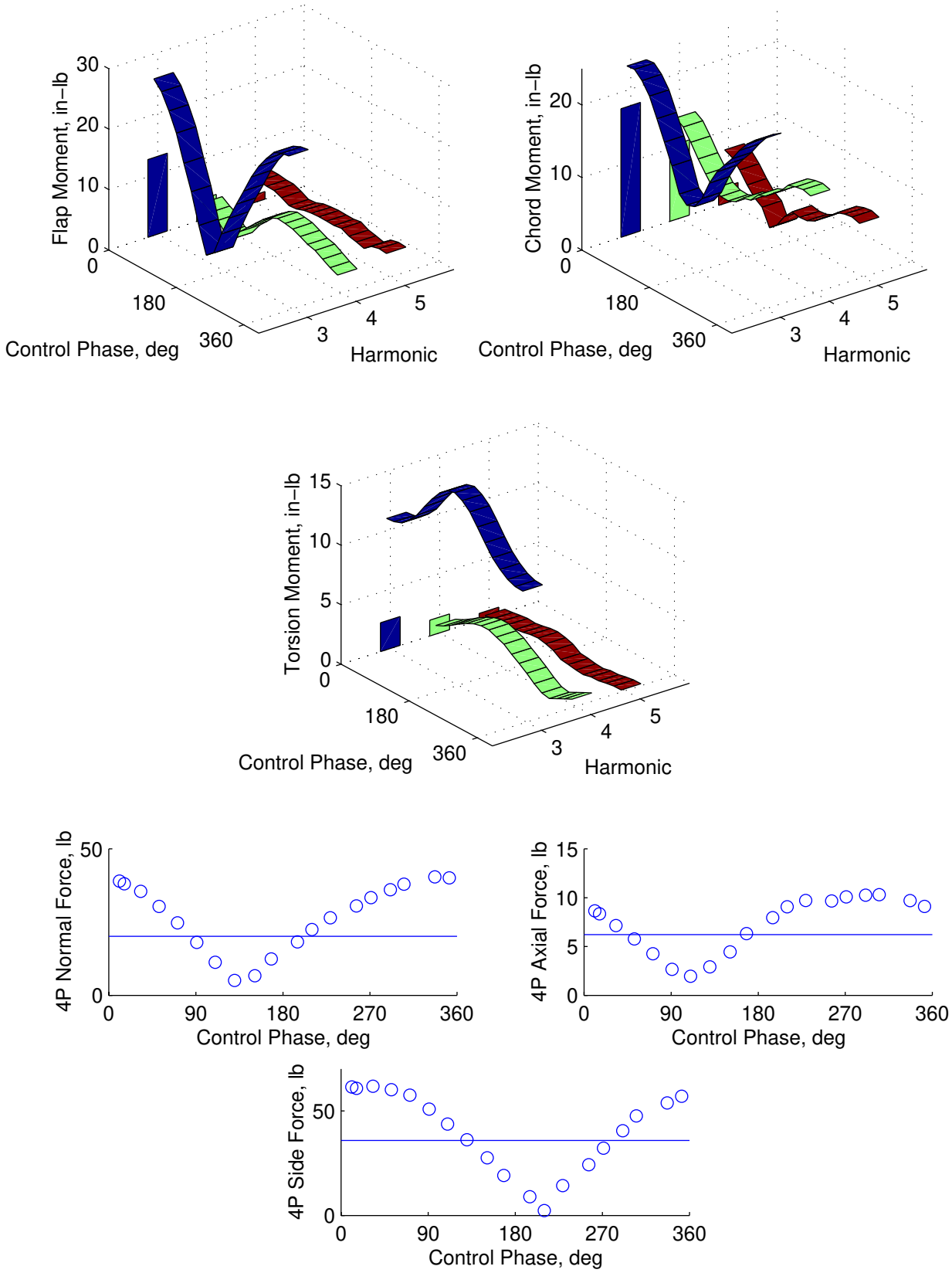

Figure 7(a). Rotating- and fixed-system loads for C_L = 0.0066, μ = 0.333, α_s = -6.0º, and 3P, 1000 V twist actuation.

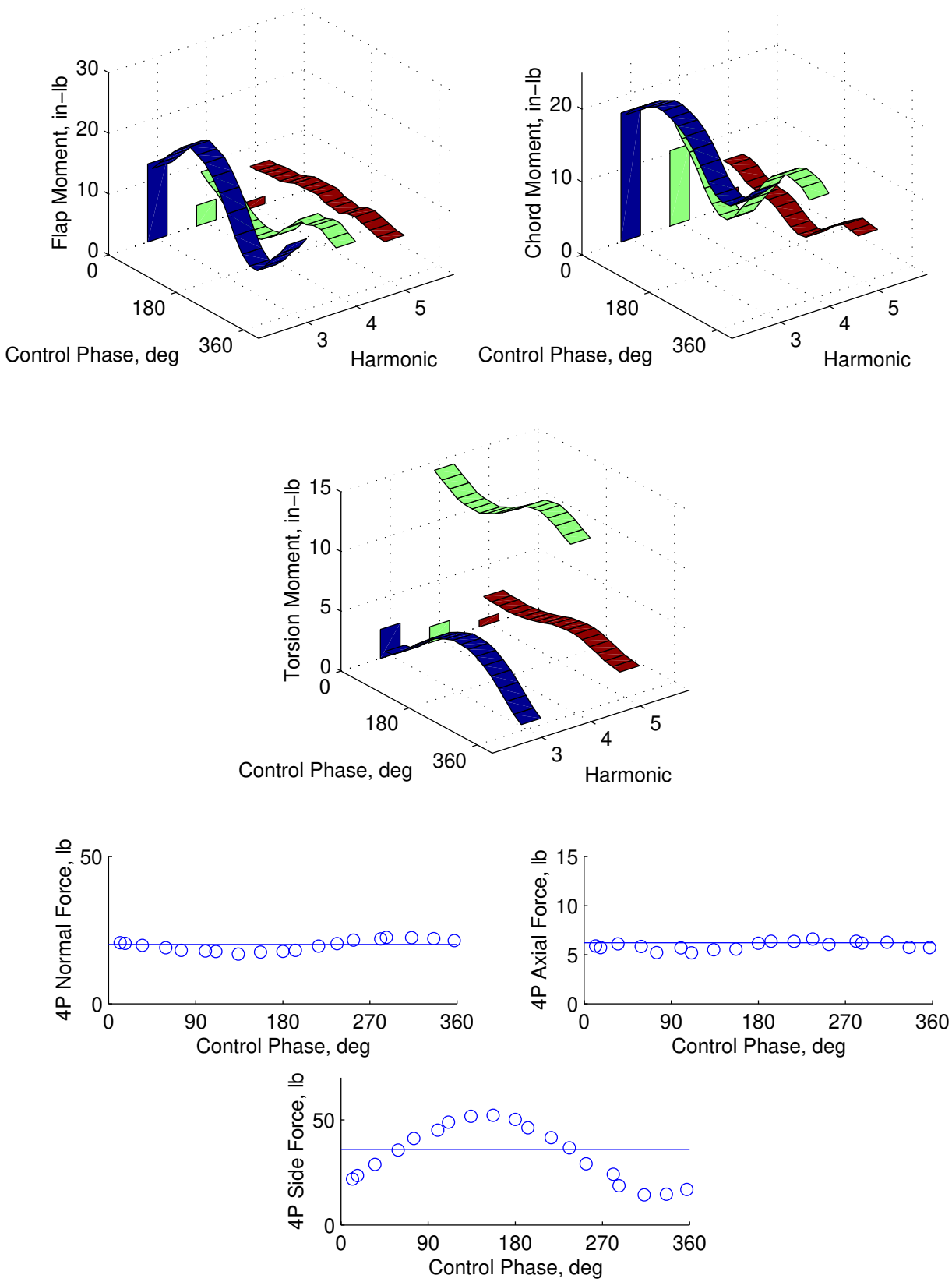

Figure 7(b). Rotating- and fixed-system loads for C_L = 0.0066, μ = 0.333, α_s = -6.0º, and 4P, 1000 V twist actuation.

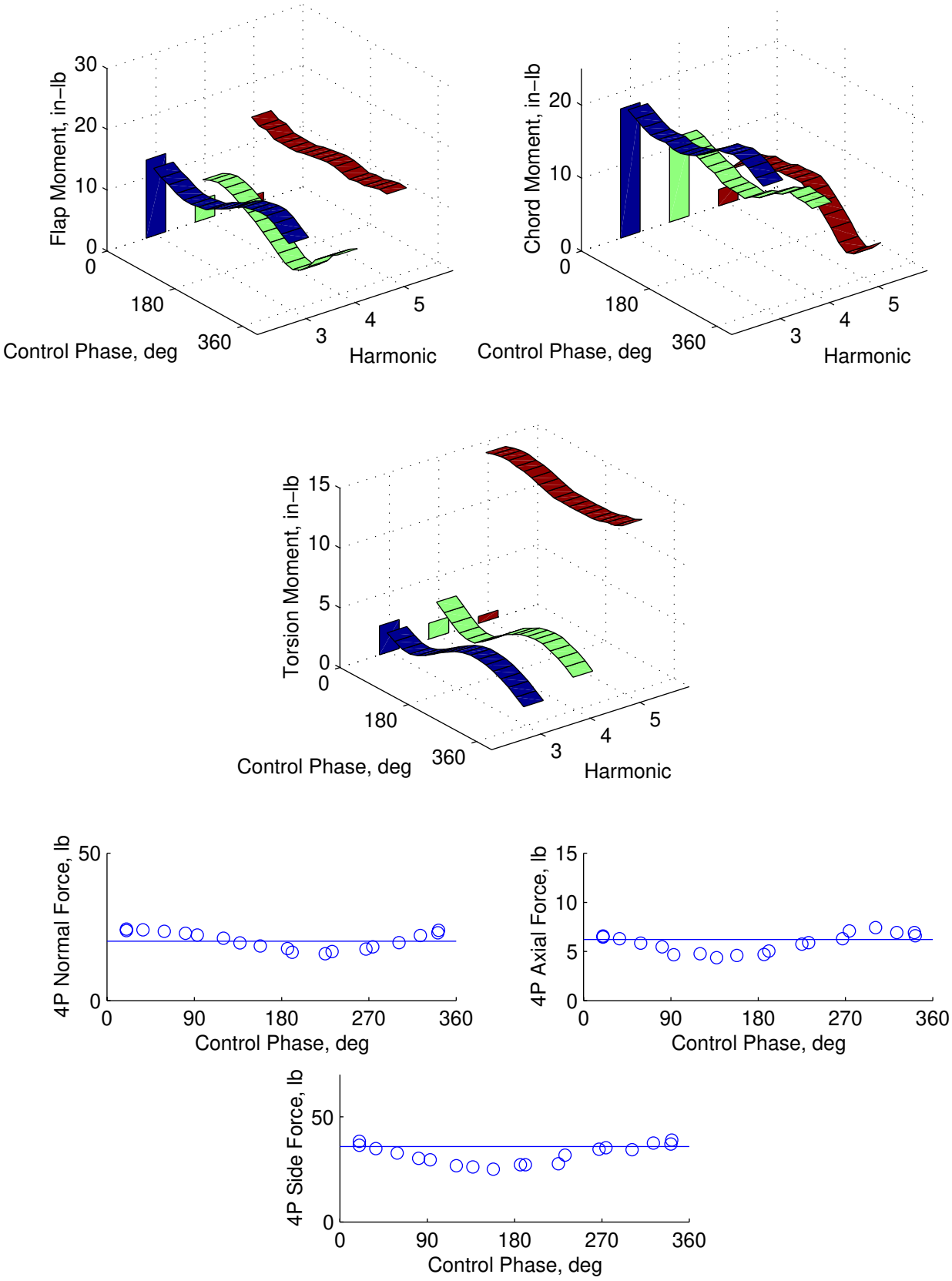

Figure 7(c). Rotating- and fixed-system loads for $C_L = 0.0066$, $\mu = 0.333$, α_s =-6.0º, and 5P, 1000 V twist actuation.

fixed-system vibratory loads reductions are noted in only the axial and side force components, where 40% and 60% reductions are evident, respectively. Large increases in 5P pitch link load are exhibited and the 4P fixed-system side force response, once again, displays characteristics of the 3P blade chord moment response.

High Advance Ratio ($\mu = 0.333$)

Figure 7(a) presents the results obtained at $C_L = 0.0066$, $\mu = 0.333$, and $\alpha_s = -6.0°$ with 3P, 1000 V amplitude active twist actuation. Pitch link results are not included due to problems encountered with the pitch link slip-ring channel at this flight condition. As for the low advance ratio case, the most pronounced effects in rotating-system loads are noted in 3P blade flap and torsion moments. The variation of the 3P torsion moment loads with twist control phase, however, is significantly more pronounced than for the low advance ratio case shown in figure 6(a) indicating a larger variation in the blade aerodynamic loading than for the low speed case. Substantial variations in 4P blade flap and chord moments are evident as well, resulting in an 80% reduction in 4P fixed-system normal force loads at a control phase of 120º to 140º. A 70% reduction in 4P fixed-system axial force is achieved at a control phase of 100º and a 95% reduction in 4P side force is evident at a control phase of 200º to 220º. As shown, however, simultaneous reduction of the fixed-system shear loads is not possible at this condition. Not presented in the figure are 4P fixed-system load reductions for pitching moment, rolling moment, and yawing moment of 90%, 60%, and 50%, respectively, at twist control phases of 160º, 180º, and 220º. As with the low speed cases, the 3P blade chord moment response appears to be the primary driver for the 4P fixed-system side force response.

Figure 7(b) presents the results obtained at $C_L = 0.0066$, $\mu = 0.333$, and $\alpha_s = -6.0°$ with 4P, 1000 V amplitude active twist actuation. The results are observed to be similar to those obtained for the low advance ratio, 4P excitation case (figure 6(b)) in that the 4P fixed-system normal force is relatively unaffected by active twist control. As before, the 4P side force is the only fixed-system shear shown to be reduced significantly and is similar in character to the 3P blade chord moment.

Figure 7(c) presents the results obtained at $C_L = 0.0066$, $\mu = 0.333$, and $\alpha_s = -6.0°$ with 5P, 1000 V amplitude active twist actuation. For this case, comparatively little fixed-system shear load reduction is noted for any active twist control phase. Of the results presented, this condition also exhibits the smallest overall variation in rotating-system loads as a function of twist control phase.

Low and High Advance Ratio Summary

The results for low- and high-speed forward flight presented in figures 6 and 7 indicate that active twist control is capable of generating significant variations in both rotating- and fixed-system loads, and that large reductions in fixed-system vibratory loads are achievable. The greatest fixed-system load reductions are evident for 3P twist excitation, even for components of the load that would traditionally be expected to respond best to 4P excitations, as for the 4P fixed-system normal force. The reasons for this phenomenon are not entirely clear at this time, however, it is noted that the 4P pitch-link loads are typically the lowest for 3P twist excitation, for all data sets examined. Conversely, 4P pitch-link loads are generally the highest when excited by 4P twist actuation, resulting in pitch-link loads roughly five times the baseline, no control levels. Generally, some of the characteristics of one or more rotating-system loads may be observed in the fixed-system responses. This is particularly true for the 3P blade chord moment and the 4P fixed-system side force, which almost always display similar trends. As expected, blade torsion loads for the harmonic at which twist actuation is being applied are always significantly higher than the baseline loads.

Full Forward-Flight Speed Range

Of considerable interest is the effect of blade twist actuation on system loads throughout the forward flight speed range. This effect is shown for the 4P root blade flapping moment and the 4P fixed-system normal force in figure 8, 9, and 10 for 1000 V twist actuation at 3P, 4P, and 5P, respectively. Figures 8 through 10 present the baseline loads as a function of advance ratio for the simulated 1g data points acquired. A high-low bar is included at each advance ratio indicating the maximum and minimum loads achieved during active twist actuation, regardless of the twist actuation control phase.

Figure 8 presents 4P load variations generated by 3P active twist actuation. As shown, significant variations in load are achievable throughout the speed range. Larger load variations are evident for blade flapping moment at the higher speeds than at the lower speeds. Load variations for the normal force are more consistent, and load reductions of 60% to 90% are shown to be achievable throughout the speed range except for $\mu = 0.267$. At this speed it was determined that the 1000 V twist actuation was larger than that required to achieve a minimum load

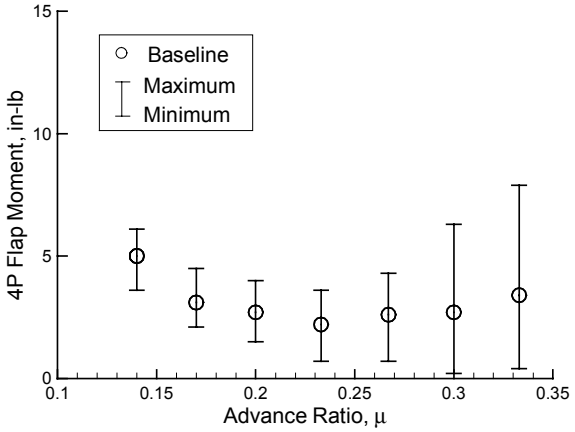

(a) Blade root flapping moment.

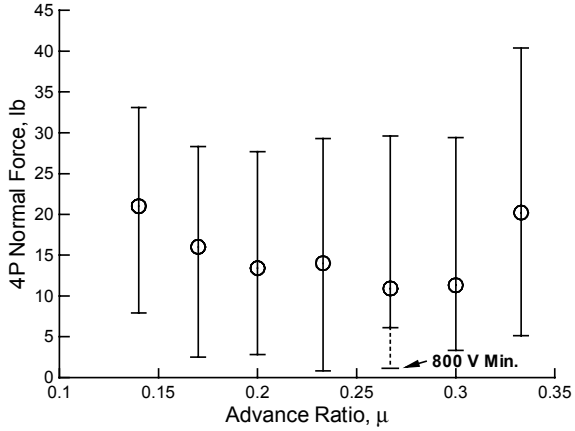

(b) Fixed-system normal force.

Figure 8. Baseline, minimum, and maximum 4P response to 3P twist actuation in forward flight. C_L = 0.0066, 1000 V actuation voltage (except where noted).

condition. As indicated on figure 8(b), the normal force load was minimized at 1.1 lb when using an 800 V twist actuation.

Figure 9 presents 4P load variations generated by 4P active twist actuation. Large load variations are evident for the blade flapping moment, however significant load reductions are achieved only at the lowest flight speeds. Small load variations are evident in the normal force with minimal load reduction across the speed range.

Figure 10 presents 4P load variations generated by 5P active twist actuation. Large load variations are evident for the blade flapping moment across the speed range. The 4P normal force is shown to be generally unresponsive to 5P twist actuation.

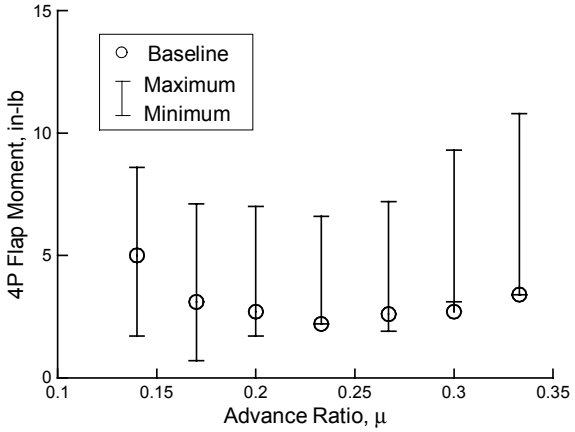

(a) Blade root flapping moment.

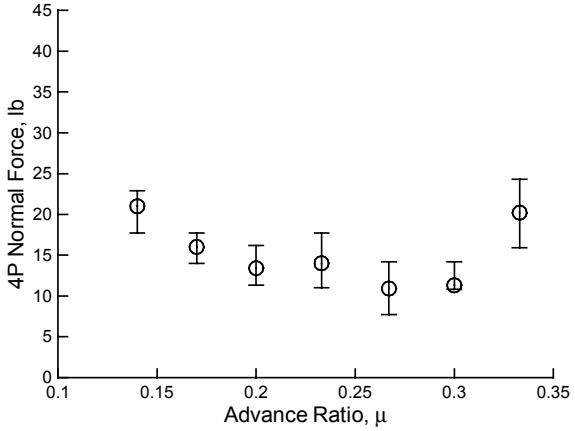

(b) Fixed-system normal force.

Figure 9. Baseline, minimum, and maximum 4P response to 4P twist actuation in forward flight. C_L = 0.0066, 1000 V actuation voltage.

PMI Blade Displacement Measurements

Figures 11 through 13 present a subset of the PMI blade displacement measurement results. These results have been used to define the sensitivity of the tip twist response to actuation frequency and voltage, and to provide a sense of the outboard flap bending moment on the blades as a function of twist actuation.

Figure 11 presents the dynamic tip twist measured in the azimuth range of 157.5º to 225.0º for 3P, 4P, and 5P twist actuation. The measurements were acquired at C_L = 0.0066, μ = 0.20, and α_s = -1.0º at a twist actuation voltage of 1000 V and twist control phase of 200º. As noted previously, the measurements are referenced to the baseline (no control) blade displacements and represent the difference in twist between the two measurements.

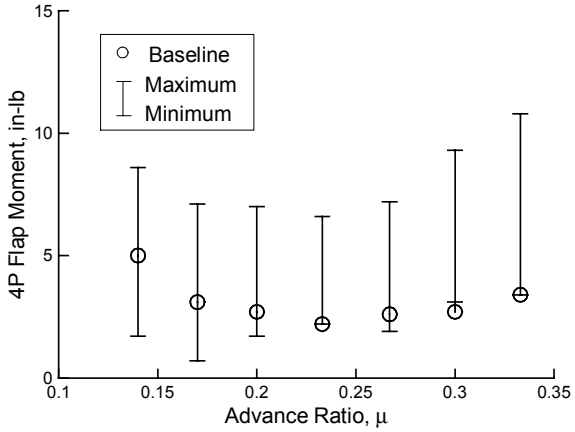

(a) Blade root flapping moment.

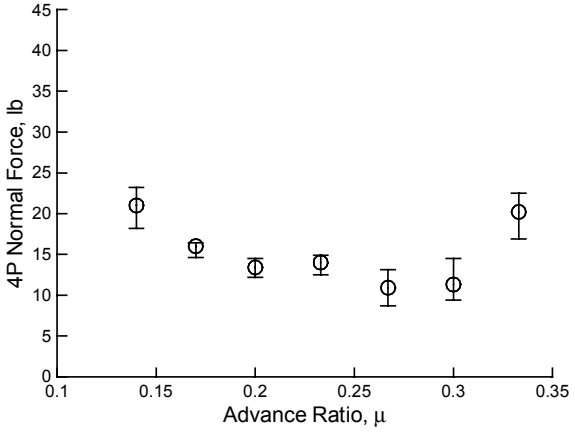

(b) Fixed-system normal force.

Figure 10. Baseline, minimum, and maximum 4P response to 5P twist actuation in forward flight. C_L = 0.0066, 1000 V actuation voltage.

As shown, twist amplitudes ranging from approximately 1.1º for 3P twist actuation, to 1.4º for 5P twist actuation are evident. These results are consistent with measurements made using the tip twist accelerometers mounted in the ATR blades.

Figure 12 presents dynamic tip twist measurements made for four different twist actuation voltage amplitudes for 3P actuation. All other conditions are identical to those presented in figure 11. As shown, tip twist actuation is somewhat of a nonlinear phenomenon due to nonlinearities evident in the strain actuation of the piezoelectric AFC actuators.

Figure 13 presents the blade bending displacements measured by the PMI system at C_L = 0.0066, μ = 0.20, and α_s = -1.0º at a twist actuation voltage of 1000 V. Active twist control phases of 40º (figure 13(a)) and 200º (figure 13(b)) are presented, representing control phases required to achieve the maximum and minimum fixed-system vibratory loads

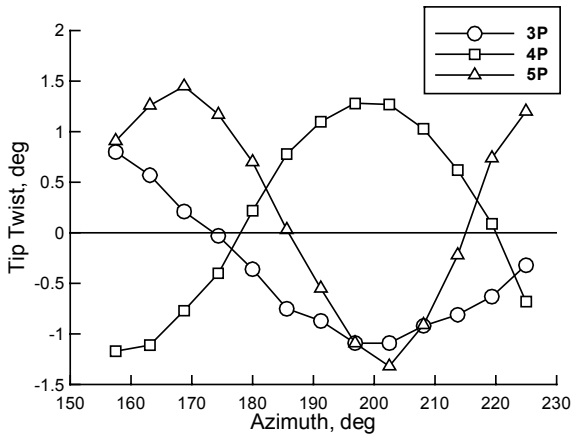

Figure 11. PMI measurement of ATR blade dynamic tip twist for 3P, 4P, and 5P twist actuation. C_L = 0.0066, μ = 0.200, and α_s = -1.0º. 1000 V actuation voltage.

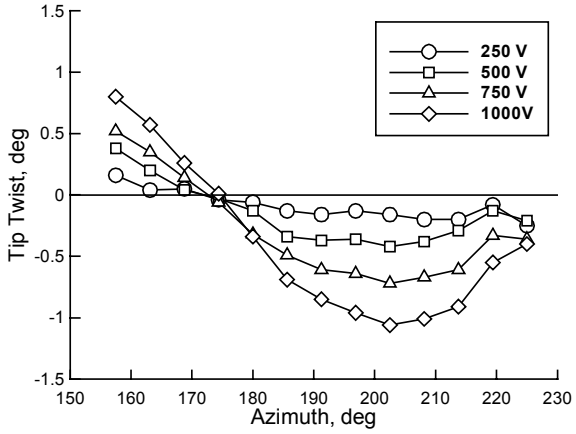

Figure 12. PMI measurement of ATR blade dynamic tip twist for varying actuation voltage amplitudes. C_L = 0.0066, μ = 0.200, and α_s = -1.0º. 3P actuation at 200º control phase.

for the flight condition. Although not entirely conclusive due to the limited results available, the figure indicates that blade flap bending moments outboard of the 30% radial station may be higher when twist actuation produces minimum fixed-system loads than when maximum fixed-system loads are produced. This is suggested by the relatively higher radius of curvature for the blade measurements taken at the 200º control phase (figure 13(b)) compared to those obtained at the 40º control phase (figure 13(a)). This result, although clearly unconfirmed at this time, is in agreement with the analytical predictions presented in reference 9 and

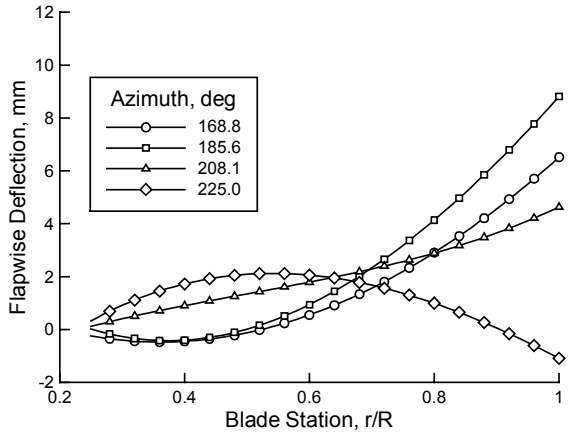

(a) Maximum fixed-system loads. 40º control phase.

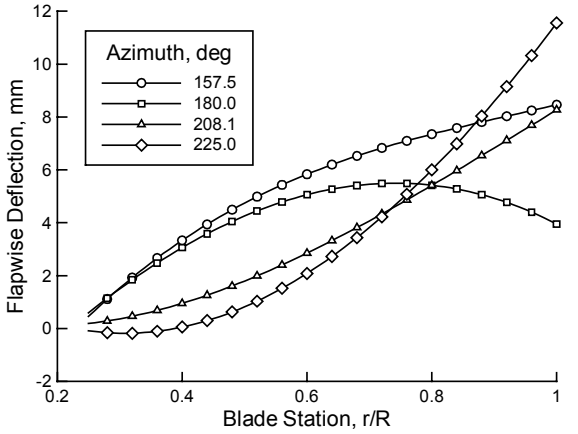

(b) Minimum fixed-system loads. 200º control phase.

Figure 13. PMI measured blade bending for maximum and minimum fixed-system load conditions. C_L = 0.0066, μ = 0.200, and α_s = -1.0º. 3P actuation at 1000 V.

would represent, along with the increasing blade torsion loads evident throughout the test data, a necessary consideration in the development of active twist rotor systems.

CONCLUSIONS

The NASA/Army/MIT Active Twist Rotor has been successfully tested in the Langley Transonic Dynamics Tunnel (TDT). The aeroelastically-scaled model rotor system, which utilizes piezoelectric active fiber composite actuators embedded in the blade for active twist control, was shown to be reliable in operation for more than 40 hours of actuated test time. The data acquired have characterized the potential vibration reduction benefits of an active twist rotor system in forward flight. Although continued research is recommended to explore more fully the potential of such rotor systems to improve rotorcraft vibrations, fundamental proof-of-concept testing has been completed showing significant promise for the technology.

Based on the results presented in this paper the following conclusions have been reached:

1. Both rotating- and fixed-system loads can be dramatically affected by changes in active twist control phase. Reductions in fixed-system loads of 60% to 95% have been demonstrated. Simultaneous reductions in all three fixed-system shear loads were observed for a low-speed flight condition (μ = 0.140). A high-speed flight condition (μ = 0.333) displayed simultaneous load reduction in two of three fixed-system shear components. An active twist control frequency of 3P was found to be the most effective in reducing fixed-system loads for both the low-speed and the high-speed conditions.

2. Active twist amplitudes of 1.1º to 1.4º are achievable for 3P to 5P twist actuation and 1000 V control amplitudes.

3. Although 4P blade loads are clearly reduced using 4P active twist control, significant increases in 4P pitch link loads tend to counter the effect in the fixed-system.

4. Large increases in torsional blade loading are evident for all active twist control cases. Limited blade displacement measurements using a non-invasive Projection Moiré Interferometry optical technique indicate that blade flap bending moments outboard of the 30% radial location may be higher when minimum vibratory loads are produced in the fixed-system.

ACKNOWLEDGEMENTS

The authors wish to acknowledge the contributions of Messrs. Gary Fleming, Hector Soto, and Scott Bartram of the NASA Langley Advanced Measurement and Diagnostics Branch for their support of the Projection Moiré Interferometry setup, measurements, and data analysis.

REFERENCES

1. Loewy, R., "Recent Developments in Smart Structures with Aeronautical Applications," *Smart Materials andStructure*s, Vol. 6, 1997, pp. 11-42.

2. Spangler, R. L., Jr. and Hall, S. R., "Piezoelectric Actuators for Helicopter Rotor Control," *AIAA/ASME/ASCE/AHS/ASC 31st Structural Dynamics and Materials Conference, Apr. 2-4, 1990, Technical Paper*s, AIAA Paper No. 90-1076, 1990, pp. 1589-1599.

3. Samak, D., Chopra, I., "A Feasibility Study to Build a Smart Rotor: Trailing Edge Flap Actuation," *SPIE Smart Structures and Materials Conference, Feb. 1-4 1993, Smart Structures and Intelligent Systems, Proceeding*s, Vol. 1917, Part 1, 1993, pp. 225-237.

4. Straub, F., "A Feasibility Study of Using Smart Materials for Rotor Control," *Proceedings of the 49th Annual Forum of the American Helicopter Societ*y, St. Louis, MO, May 1993.

5. Millot, T., Friedmann, P., "Vibration Reduction in Helicopter Rotors Using an Actively Controlled Partial Span Trailing Edge Flap Located on the Blade," NASA Contractor Report 4611, June 1994.

6. Giurgiutiu, V., Chaudhry, Z., Rogers, C., "Engineering Feasibility of Induced Strain Actuators for Rotor Blade Active Vibration Control," *Journal of Intelligent Material Systems and Structure*s, Vol. 6, No. 5, September 1995, pp. 583-597.

7. Fulton, M., Ormiston, R., "Hover Testing of a Small-Scale Rotor with On-Blade Elevons," Presented at the American Helicopter Society 53rd Annual Forum, Virginia Beach, VA, April 29-May 1, 1997.

8. Fulton, M., "Design of the Active Elevon Rotor for Low Vibration," Presented at the American Helicopter Society Aeromechanics Specialists Meeting, Atlanta, GA, November 13-15, 2000.

9. Derham, R., "The Aeromechanics of (Smart) Active Rotors," Presented at the American Helicopter Society Aeromechanics Specialists Meeting, Atlanta, GA, November 13-15, 2000.

10. Barrett, R., "Intelligent Rotor Blade Structures Development Using Directionally Attached Piezoelectric Crystals," M.S. thesis, University of Maryland, College Park, MD, 1990.

11. Chen, P., and Chopra, I., "A Feasibility Study to Build a Smart Rotor: Induced Strain Actuation of Airfoil Twisting Using Piezoceramic Crystals," *SPIE Smart Structures and Materials Conference, Feb. 1-4 1993, Smart Structures and Intelligent Systems, Proceeding*s, Vol. 1917, Part 1, 1993, pp. 238-254.

12. Derham, R., and Hagood, N., "Rotor Design Using Smart Materials to Actively Twist Blades," *Proceedings of the American Helicopter Society 52nd Annual Forum*, Vol. 2, Washington, D.C., June 4-6, 1996, pp. 1242-1252.

13. Wilkie, W. Keats, "Anisotropic Piezoelectric Twist Actuation of Helicopter Rotor Blades: Aeroelastic Analysis and Design Optimization," Ph. D. thesis, University of Colorado, Boulder, CO, 1997.

14. Rodgers, J. P., Hagood, N. W., "Development of an Integral Twist-Actuated Rotor Blade for Individual Blade Control," AMSL Report #98-6, Active Materials and Structures Laboratory, Massachusetts Institute of Technology, October 1998.

15. Wilkie, W. K., Wilbur, M. L., Mirick, P. H., Cesnik, C. E. S., and Shin, S. J., "Aeroelastic Analysis of the NASA/Army/MIT Active Twist Rotor," *Proceedings of the American Helicopter Society 55th Annual Forum*, Montreal, Canada, May 25-27, 1999.

16. Cesnik, C. E. S., Shin, S. J., Wilkie, W. K., Wilbur, M. L., and Mirick, P. H., "Modeling, Design, and Testing of the NASA/Army/MIT Active Twist Rotor Prototype Blade," *Proceedings of the American Helicopter Society 55th Annual Forum*, Montreal, Canada, May 25-27, 1999.

17. Shin, SangJoon, Cesnik, Carlos E. S., "Design, Manufacturing and Testing of an Active Twist Rotor," AMSL Report #99-3, Active Materials and Structures Laboratory, Massachusetts Institute of Technology, June 1999.

18. Wilbur, M. L., Yeager, W.T., Jr., Wilkie, W. K., Cesnik, C. E. S., and Shin, S. J., "Hover Testing of the NASA/Army/MIT Active Twist Rotor Prototype Blade," *Proceedings of the American Helicopter Society 56th Annual Forum*, Virginia Beach, VA, May 2-4, 2000.

19. Shin, S. J., Cesnik, C. E. S., and Wilbur, M. L., "Dynamic Response of Active Twist Rotor Blades," *AIAA/ASME/ASCE/AHS/ASC 41st*

Structures, Structural Dynamics and Materials Conference, 2000, Technical Papers, AIAA Paper No. 2000-1711, 2000.

20. Bent, A., Hagood, N., "Improved Performance in Piezoelectric Fiber Composites Using Interdigitated Electrodes," SPIE Smart Structures and Materials Conference, February 27-28 1995, *Smart Materials, Proceedings*, Vol. 2441, 1995, pp. 196-212.

21. Yeager, W. T., Jr., Mirick, P. H., Hamouda, M-N., Wilbur, M. L., Singleton, J. D., Wilkie, W. K., "Rotorcraft Aeroelastic Testing in the Langley Transonic Dynamics Tunnel," *Journal of the American Helicopter Society*, Vol. 38, No. 3, July 1993, pp.73-82.

22. Fleming, G. A., Soto, H. L., South, B. W., Bartram, S. M., "Advances in Projection Moiré Interferometry Development for Large Wind Tunnel Applications," Paper No. 1999-01-5598, Presented at the *SAE 1999 World Aviation Congress and Exposition*, San Francisco, CA, October 19-21, 1999.